PHILOSOPHICAL TRANSACTIONS OF THE ROYAL SOCIETY A MATHEMATICAL, PHYSICAL & ENGINEERING SCIENCES

Plastic flow, microstructure evolution, and defect formation during primary hot working of titanium and titanium aluminide alloys with lamellar colony microstructures

S.L. Semiatin, V. Seetharaman and A.K. Ghosh

Phil. Trans. R. Soc. Lond. A 1999 **357**, 1487-1512
doi: 10.1098/rsta.1999.0386

THE ROYAL SOCIETY

Plastic flow, microstructure evolution, and defect formation during primary hot working of titanium and titanium aluminide alloys with lamellar colony microstructures

By S. L. Semiatin[1], V. Seetharaman[2] and A. K. Ghosh[3]

[1]*Air Force Research Laboratory, Materials and Manufacturing Directorate, AFRL/MLLM, Wright-Patterson Air Force Base, OH 45433, USA*
[2]*Materials and Processes Division, UES Inc., Dayton, OH 45432, USA*
[3]*Department of Materials Science and Engineering, The University of Michigan, Ann Arbor, MI 48109, USA*

Plastic flow response, microstructure evolution, and defect formation during the primary hot working of conventional alpha/beta titanium alloys and gamma titanium aluminide alloys with two-phase lamellar colony microstructures are reviewed. The effects of initial grain/colony size, deformation rate and temperature on constitutive behaviour and the mechanisms associated with the observed flow softening are discussed. The kinetics of dynamic globularization are summarized and interpreted in terms of measured constitutive response. In addition, the mechanisms underlying failure via shear localization and cavitation during breakdown metalworking operations are described.

Keywords: titanium alloys; titanium aluminide alloys; constitutive behaviour; ingot breakdown; shear band formation; cavitation

1. Introduction

The primary hot working of engineering alloys plays a key role in the control of microstructure and, thus, final properties. As such, the phenomenology and mechanisms underlying dynamic phase and microstructural transformations have received considerable attention (Jonas & McQueen 1975). Because of the industrial and commercial significance of steel and aluminium alloys, research and understanding of these material groups have progressed farthest (Sellars 1990; Laasraoui & Jonas 1991; Humphreys & Hatherly 1995). For example, the mechanisms of dynamic recovery, discontinuous and continuous dynamic recrystallization, and various static restorative processes following hot working are well documented for a variety of nominally single-phase alloys (e.g. carbon–manganese steels) and particle-containing alloys (e.g. high-strength low-alloy steels; aluminium alloys). In addition, the last decade has seen substantial work in the area of modelling of such processes, chiefly using numerical approaches such as the Monte Carlo and cellular automaton techniques (Rollett 1997; Rollett *et al*. 1992; Goetz & Seetharaman 1998).

Research on microstructure evolution and failure during primary hot working of high-temperature aerospace alloys, such as those based on nickel and titanium, has been less extensive. The phenomenology and mechanism of dynamic recrystallization during hot deformation of nickel-based superalloys have been documented for

both supersolvus and subsolvus regimes (Kaibyshev *et al*. 1993; Shen *et al*. 1995). Similarly, the flow characteristics and (continuous) dynamic recrystallization that pertain to the hot working of single-phase beta titanium alloys have been investigated (Weiss & Semiatin 1998). On the other hand, the behaviour of two-phase alpha/beta titanium alloys during bulk forming, particularly during the breakdown of the lamellar colony microstructure at temperatures below the beta transus (the temperature below which beta → alpha + beta) has been documented to a lesser extent.

The height reductions for the dynamic globularization of the colony microstructure during subtransus hot working of alloys such as Ti–6Al–2Sn–4Zr–2Mo (weight per cent) have been determined using compression testing (Semiatin *et al*. 1983; Malcor *et al*. 1985).† Unfortunately, the strain non-uniformity inherent in compression, even under nominally well-lubricated isothermal conditions (Oh *et al*. 1992), was not taken into consideration in the interpretation of these measurements and, thus, lessens their quantitative usefulness. Other work has shown that strain path can also have a major influence on globularization kinetics (E. Rauch *et al*. 1982, unpublished research; Korshunov *et al*. 1994). For example, it has been found that monotonic types of deformation (e.g. torsion, tension) produce noticeably more rapid globularization rates than the non-monotonic modes (e.g. reversed torsion). With respect to transformation mechanisms, Weiss *et al*. (1985) have suggested that dynamic globularization is preceded by the formation of intense shear bands within the alpha lamellae. The formation of such high-energy alpha/alpha interfaces in contact with beta platelets was postulated to give rise to surface-tension-driven penetration of the alpha plates by the beta phase.

The failure of alpha/beta titanium alloys with lamellar colony microstructures during primary hot working has been shown to be usually one of two types: cavitation-controlled ductile failure or shear localization (Semiatin *et al*. 1997). Cavitation-failure results from the initiation of cavities at prior-beta grain boundaries due to the development of secondary tensile stresses during bulk forming. Although several investigators have attempted to quantify cavitation through measurements of hot tensile ductility (Matsumoto *et al*. 1985; Suzuki & Eylon 1993), relatively little effort has been expended to describe the detailed mechanisms of cavity initiation and growth, let alone to establish the effect of stress state on such failure phenomena (Semiatin *et al*. 1998*b*). In contrast, shear localization has been extensively studied (Semiatin & Jonas 1984). The influence of material variables (e.g. flow-softening rate, strain-rate sensitivity) and process parameters (e.g. die temperature, strain rate/contact time) on localization tendencies during both isothermal and conventional (non-isothermal) processes has been elucidated.

The objective of the present paper is to summarize recent research on plastic flow, microstructure evolution, and fracture behaviour during bulk hot working of alpha/beta titanium alloys with colony microstructures. These results are compared with similar observations for the hot working of near-gamma titanium aluminide alloys with lamellar colony microstructures. Extensive research is now being conducted to extend conventional hot-working practices to these intermetallic materials (Semiatin *et al*. 1997); thus, it is important to determine the similarities and differ-

† The term globularization, rather than recrystallization, is used in the present context to indicate the spheroidization of colony alpha plates because of the uncertainty of the precise mechanism that is operative.

ences between the hot-working behaviour of the two alloy groups. Future research efforts that would help complete our understanding of these materials are also summarized.

2. Materials

The majority of the following discussion focuses on the alpha/beta titanium alloy, Ti–6Al–4V (weight per cent), and the near-gamma titanium aluminide alloy, Ti–45.5Al–2Cr–2Nb (atomic per cent). For both alloys, a lamellar microstructure is formed by slow-to-moderate cooling from a high-temperature field (beta for Ti–6Al–4V, alpha for Ti–45.5Al–2Cr–2Nb) through a two-phase field (alpha + beta for Ti–6Al–4V, alpha + gamma for Ti–45.5Al–2Cr–2Nb). The lamellar microstructures thus produced comprise colonies of alternating lamellae of hexagonal close-packed (HCP) alpha and BCC beta (Ti–6Al–4V) or HCP alpha/ordered alpha-two and ordered face-centred tetragonal (FCT) gamma (Ti–45.5Al–2Cr–2Nb). The gamma alloy also contains a small percentage of the ordered BCC (B2) phase.

The lamellar microstructures can often be found in cast ingots of the titanium and titanium aluminide alloys. However, the work reported herein made use of wrought fine-grain starting materials that were given special short-time heat treatments in order that microstructural features such as prior-beta or prior-alpha grain size could be carefully controlled. For the Ti–6Al–4V alloy, samples with a 400 μm prior-beta grain size and 200 μm colony size, containing *ca.* 1 μm thick alpha plates and a 3 μm thick layer of grain-boundary alpha, were produced via heat treatment of hot-rolled bar stock at 955 °C/10 min + 1040 °C/12 min + 815 °C/10 min + air cool (figure 1*a*) (Semiatin *et al.* 1998*b*). The beta transus temperature of the alloy was 995 °C. The Ti–6Al–4V exhibited a relatively strong alpha-phase texture (*ca.* 7 × random) with two major components: one with the basal poles parallel to the bar axis; and one with the basis poles rotated *ca.* 30° from the transverse (radial) direction toward the bar axis (figure 1*b*). Although only touched on briefly below, a second lot of this material with a 100 μm prior-beta grain size, 50 μm colony size, and an almost identical texture, produced via a similar short-time heat treatment, was also used. For the Ti–45.5Al–2Cr–2Nb alloy, samples with alpha grain/lamellar colony sizes between 80 and 900 μm containing 1 μm thick lamellae were obtained using a heat treatment of 1260 °C/30 min + 1321 °C/0–60 min + cool 1321 °C → 900 °C at 10–15 °C min^{-1} + air cool (figure 2). The alpha transus temperature (temperature at which alpha → alpha + gamma) for this alloy was 1300 °C. Samples with fine grain/colony sizes (less than *ca.* 200 μm) also had a small volume fraction of intergranular gamma particles.

The plastic flow, microstructure evolution and fracture behaviour of the two alloys were characterized using constant strain rate, isothermal hot-compression tests and constant crosshead speed hot-tension tests. The interpretation of both the compression and tension results was facilitated using finite-element method (FEM) modelling (Oh *et al.* 1992; Lombard *et al.* 1993).

3. Plastic flow and microstructure evolution: Ti–6Al–4V

The behaviour of Ti–6Al–4V with a colony preform microstructure during subtransus hot working is discussed in terms of flow curves, deformation mechanisms/constitutive behaviour, and flow-softening behaviour/microstructure evolution established from hot compression tests.

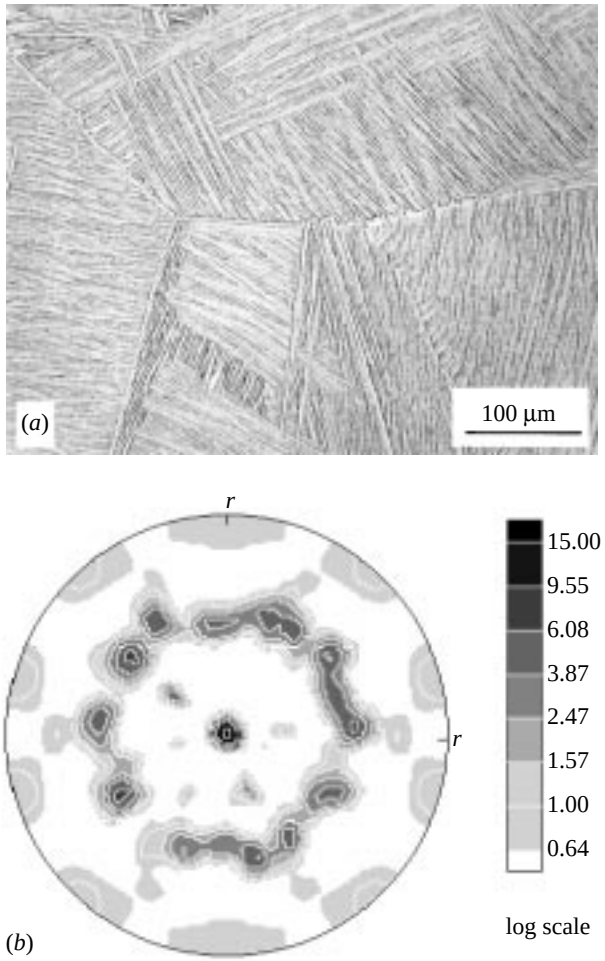

Figure 1. Ti–6Al–4V with a lamellar colony microstructure: (*a*) optical microstructure; (*b*) (0002) pole figure for the alpha phase.

(*a*) *Flow curves*

Measured true stress–true strain (flow) curves for Ti–6Al–4V with the 400 µm prior-beta grain size are summarized in figure 3. All of the curves exhibit a peak flow stress at relatively low strains (less than about 0.03) followed by moderate to extensive flow softening. The overall degree of flow softening is comparable at 815 °C and 900 °C, but slightly less at 955 °C. Furthermore, all of the flow curves tend to exhibit a noticeably lower rate of flow softening at strains of the order of 0.7. Flow curves for Ti–6Al–4V with a 100 µm prior-beta grain size (not shown) are essentially identical to those for the 400 µm grain-size material.

(*b*) *Constitutive behaviour/deformation mechanisms*

The absence of a grain/colony size dependence of the flow stress suggests that plastic flow is controlled by the glide and climb of dislocations (Frost & Ashby 1982).

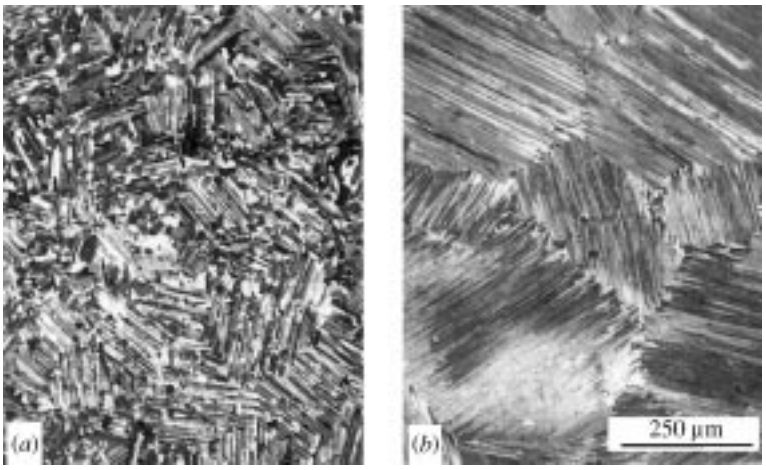

Figure 2. Polarized light micrographs of Ti–45.5Al–2Cr–2Nb with lamellar colony/grain sizes of (*a*) 200 μm or (*b*) 600 μm.

This conclusion can be rationalized on the basis of the relatively coarse grain/colony sizes and, hence, the limited contribution of grain-boundary-sliding-type processes to the deformation.

An analysis of the peak flow stress data and measurements of the strain-rate sensitivity ('m' value) as a function of strain support this conclusion. The values of m at the strain $\bar{\varepsilon}_{\mathrm{p}}$ corresponding to the peak stress $\bar{\sigma}_{\mathrm{p}}$ reveal a slight increase with increasing temperature and decreasing strain rate (table 1). In all cases, however, $m(\bar{\varepsilon}_{\mathrm{p}})$ is between 0.06 and 0.22. Because of the variation of m_{p} with strain rate and, hence, the breakdown of power-law creep at high strain rates, the relation between strain rate $\dot{\bar{\varepsilon}}$ and $\bar{\sigma}_{\mathrm{p}}$ was also fitted using the classical hyperbolic sine relation (Jonas *et al*. 1969), even though this relation is usually applied to describe the steady-state flow of single-phase alloys:

$$\dot{\bar{\varepsilon}} = A[\sinh(\alpha\bar{\sigma}_{\mathrm{p}})]^n, \tag{3.1}$$

in which A, α and n are constants. The fit of equation (3.1) to the data for Ti–6Al–4V with colony microstructure is shown in figure 4. All of the data are well fit using $\alpha = 0.008\ \mathrm{MPa}^{-1}$; the values of A were 3.82×10^{-5}, 1.38×10^{-3} and $9.22 \times 10^{-2}\ \mathrm{s}^{-1}$ at 815, 900 and 955 °C, respectively. Values of the stress exponent n were 3.36, 3.65 and 4.73 at the three temperatures. This finding of $n \approx 4$ over the entire strain rate and temperature range supports the conclusion that plastic flow is controlled by dislocation glide/climb processes (Frost & Ashby 1982; Courtney 1990).

The peak flow stress data can also be fitted by an expression of the form $Z \sim A(\sinh\alpha\bar{\sigma})^{n'}$, where Z denotes the Zener–Hollomon parameter $\dot{\bar{\varepsilon}}\exp(Q/RT)$, Q is an apparent activation energy, R is the gas constant, and T is temperature. For the Ti–6Al–4V peak flow stress results shown in figure 3, $Q \approx 700\ \mathrm{kJ\ mol}^{-1}$ and $n' = 3.86$ provides a reasonably good fit. (A similar fit using $Q \approx 700\ \mathrm{kJ\ mol}^{-1}$ and $n' = 4.34$ pertains to the flow stress data at $\boldsymbol{\varepsilon} = 0.5$.) The activation energy of $700\ \mathrm{kJ\ mol}^{-1}$ does not have a true physical significance, but is rather an artifact of the fitting of data for two-phase materials whose phase proportions vary greatly with temperature (Briottet *et al*. 1996).

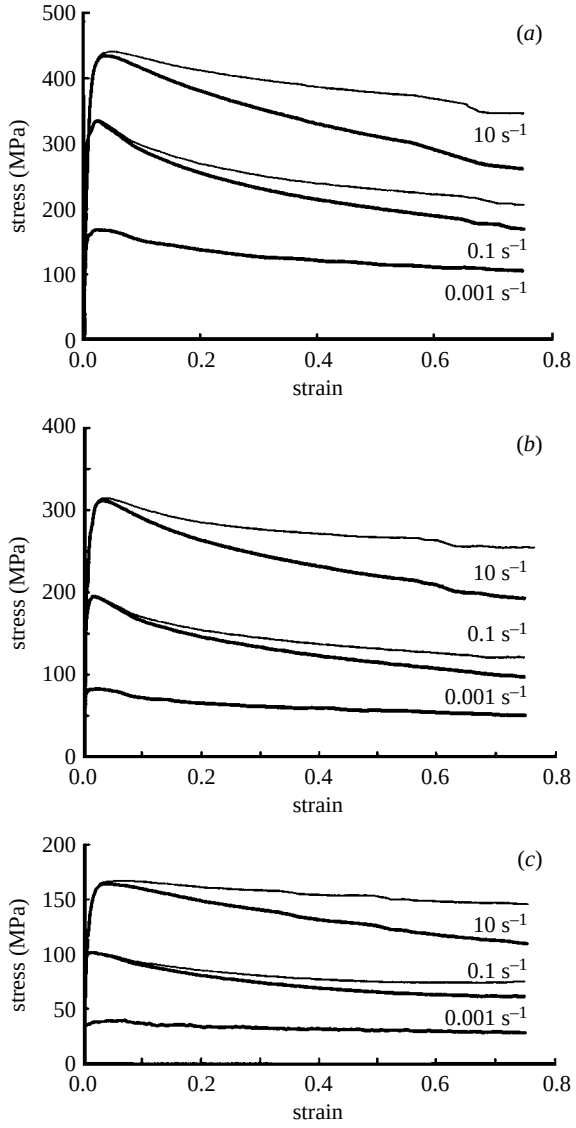

Figure 3. Measured (thick lines) and 'temperature-corrected' (thin lines) flow curves for Ti–6Al–4V from hot compression tests at 0.001, 0.1 and 10 s^{-1} and test temperatures of (*a*) 815 °C, (*b*) 900 °C, and (*c*) 955 °C.

Strain-rate jump testing reveals an increase of the rate sensitivity m with strain (figure 5). The increase is most noticeable for tests at 815 °C and 900 °C. Despite such increases, these rate sensitivity measurements still lay in a deformation regime that would be characterized by creep-type behaviour, i.e. $m \approx 0.25$.

(*c*) *Flow-softening behaviour/microstructure evolution*

The flow softening observed in flow curves for the Ti–6Al–4V alloy (figure 3) may be hypothesized to arise from several possible sources. These include deformation

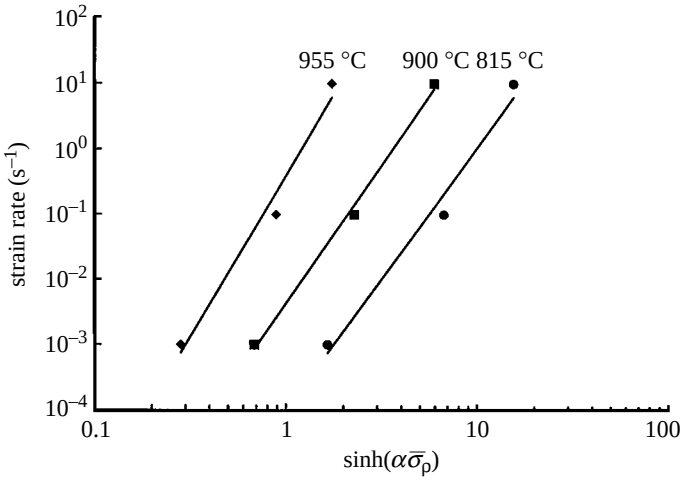

Figure 4. Log–log plot of strain rate $\dot{\bar{\varepsilon}}$ versus $\sinh(\alpha\bar{\sigma}_{\mathrm{p}})$ from hot compression data for Ti–6Al–4V.

Table 1. *Strain-rate sensitivity data determined from peak stresses of continuous* Ti–6Al–4V *flow curves*

(Ti–6Al–4V with a lamellar colony microstructure.)

	$m(\bar{\varepsilon}_{\mathrm{p}})$ at $\dot{\bar{\varepsilon}} =$	
temperature (°C)	10^{-3}–10^{-1} s^{-1}	10^{-1}–10^{1} s^{-1}
815	0.148	0.058
900	0.183	0.101
955	0.218	0.105

heating (at higher strain rates) or changes in microstructure morphology, substructure or texture.

(i) *Flow softening due to deformation heating*

The magnitude of the influence of deformation heating on flow softening may be ascertained using the procedure described by Semiatin & Lahoti (1981). This method assumes that the flow stress at a given strain rate is a function of strain and *instantaneous* temperature. So-called 'temperature-corrected' flow curves are compared to measured ones in figure 3. The temperature-corrected flow stresses were most different from the measured ones at high strain rates (e.g. 10 s^{-1}), due to near-adiabatic conditions, and at low temperatures at which flow stress levels and the temperature dependence of the flow stress are quite high. For $\dot{\bar{\varepsilon}} = 10^{-3}$ s^{-1}, adequate time is available for essentially all deformation-induced heating to dissipate into the dies, and, thus, the temperature correction is negligible.

The accuracy of this method of compensating for deformation heating has been evaluated by conducting hot compression tests that are interrupted for a short time-interval (*ca.* 10–20 s) at $\varepsilon \sim 0.5$. The interruption allows deformation-induced heat

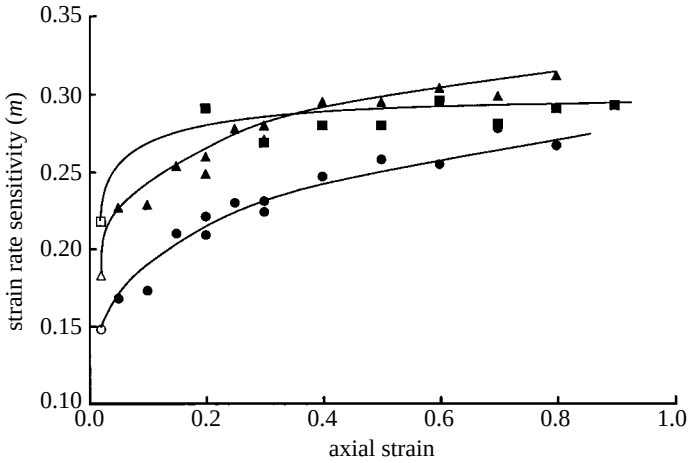

Figure 5. Variation of the strain-rate sensitivity m for Ti–6Al–4V as a function of strain determined from 'jump' tests conducted at strain rates of 0.02 and 0.1 s^{-1}. •, 815 °C; ▲, 900 °C; ■, 955 °C. Open data points: m based on peak flow stress values.

Table 2. *Flow-softening behaviour of* Ti–6Al–4V
(Ti–6Al–4V with a lamellar colony microstructure.)

		$\Delta\bar{\sigma}/\bar{\sigma}_p$ at $\boldsymbol{\varepsilon} = 0.50$		
temperature (°C)	strain rate (s^{-1})	heating-related softening	non-heating softening	total softening
815	10^{-3}	0.00	0.26	0.26
815	10^{-1}	0.09	0.29	0.38
815	10^{1}	0.16	0.12	0.28
900	10^{-3}	0.00	0.23	0.23
900	10^{-1}	0.11	0.31	0.40
900	10^{1}	0.15	0.13	0.28
955	10^{-3}	0.00	0.16	0.16
955	10^{-1}	0.10	0.23	0.33
955	10^{1}	0.17	0.05	0.22

to dissipate into the dies and the sample temperature to re-equilibrate to the initial test temperature. The results of such tests have indicated that, indeed, the flow stress on reloading (i.e. after the temperature has dropped back to the initial test temperature) does come very close to that of the temperature-corrected flow curve.

The corrected and uncorrected flow curves in figure 3 provide a convenient semi-quantitative means of characterizing the flow softening due to heating effects and that due to changes in microstructure. This has been accomplished by estimating the value of $\Delta\bar{\sigma}/\bar{\sigma}_p$ at an axial strain of 0.50, namely

$$\Delta\bar{\sigma}/\bar{\sigma}_p = (\bar{\sigma}_p - \bar{\sigma}(0.50))/\bar{\sigma}_p.$$

When $\bar{\sigma}(0.50)$ is taken from the measured or temperature-corrected flow curves,

$\Delta\bar{\sigma}/\bar{\sigma}_{\mathrm{p}}$ gives a measure of the total or the microstructure-related softening, respectively (table 2). The level of the heating-related softening, or the difference between these two quantities, increases with strain rate and is, essentially, independent of temperature for a given strain rate.

(ii) *Flow softening due to dislocation substructure effects*

The microstructure-related softening values for Ti–6Al–4V with the lamellar colony microstructure are comparable for $10^{-3}\,\mathrm{s}^{-1}$ and $10^{-1}\,\mathrm{s}^{-1}$, but considerably greater than those for the $10\,\mathrm{s}^{-1}$ tests (table 2). One of the principal sources of non-heating-related flow softening, which may also be useful in explaining the rate dependence of such softening, is dislocation substructure development. The gradual increase of m value with strain (figure 5), particularly at the two lower test temperatures at which the level of flow softening is greater, suggests the development of a softer substructure such as subgrains within the alpha lamellae, as was observed by Weiss *et al*. (1985). However, the formation of substructure, the occurrence of dynamic recrystallization, etc., are often controlled by thermally activated processes. For example, the strain for the onset of dynamic recrystallization in single-phase metals is a strong function of strain rate and temperature (Jonas & McQueen 1975). By contrast, the present flow curves (figure 3) exhibit strains for the peak stress and the onset of flow softening that are very low (less than about 0.03) and show no discernible dependence on strain rate and temperature. Moreover, it should be emphasized that both single-phase alpha and single-phase beta titanium with equiaxed grain morphologies undergo dynamic recovery, develop subgrain structures, and exhibit steady-state flow without flow softening during hot working (Weiss & Semiatin 1998, 1999).

Further evidence that substructure evolution contributes little to the observed flow softening is provided from other interrupted hot compression tests. In these experiments, the hold comprised a 30 min anneal at 900 °C to effect static recovery/annihilation of dislocations. In all cases, the flow curve on reloading lay close to the temperature-corrected flow curve at the strain corresponding to that at the end of the first 'hit' (figure 6). Metallographic examination of the final microstructure in such samples (which were compressed to a total strain of 0.5) revealed no evidence of globularization. Thus, it might be conjectured that a 'permanent' level of softening has been imposed during deformation that arises from neither substructure nor microstructure changes *per se*. However, detailed transmission electron microscopy (TEM) studies are needed to illuminate such details further.

(iii) *Flow softening due to microstructure morphology changes*

Changes in microstructure morphology can be one of two types, globularization of the lamellar colonies and platelet bending/kinking. The absence of globularization at low strains suggests that, by and large, such a process is not responsible for the observed flow softening. On the other hand, platelet bending and kinking (figure 7*a*) does occur at low strains. This latter phenomenon may be a form of plastic buckling analogous to that which occurs during compression of beams (Nadai 1950). The plastic buckling of a beam results in a peak load and a noticeable load drop. The constrained deformation of a lamellar colony microstructure is somewhat more complex, but certainly warrants further study as a source of flow softening.

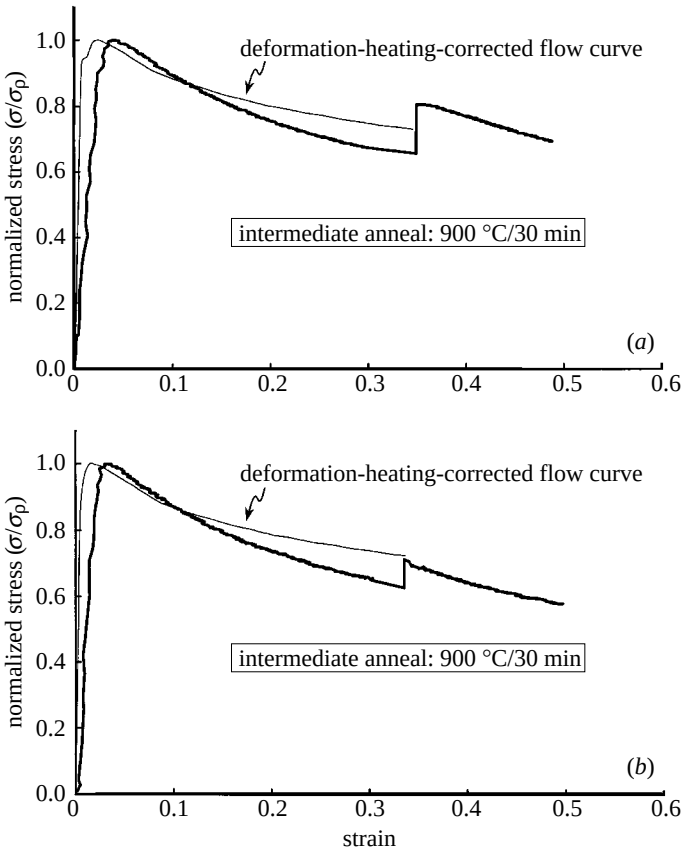

Figure 6. Comparison of flow curves from 'two-hit' hot compression tests conducted on Ti–6Al–4V and the corresponding curves from *uninterrupted* experiments at a strain rate of $0.1\ s^{-1}$ and test temperatures of (*a*) 815 °C or (*b*) 900 °C. In both interrupted tests, a static dwell of 30 min at 900 °C was imposed between 'hits'.

Careful examination of optical micrographs reveals that globularization initially occurs at the 'kinks' in the lamellae and along the prior-beta grain boundaries (figure 7*a*); at higher strains, however, globularization proceeds more or less uniformly with no preference for grain boundaries. Quantitative metallography, coupled with FEM results to determine local strain non-uniformities, shows that the strain for 'initiation' of dynamic globularization is approximately 0.75–1.0, and that for completion it is of the order of 2.0–2.5, irrespective of strain rate and temperature. Representative plots of fraction globularized as a function of strain (for deformation at $0.001\ s^{-1}$) are shown in figure 7*b*. The plots indicate a relatively weak dependence on temperature, despite the large change in volume fraction of alpha over this temperature range (Cope & Ridley 1986) and the concomitant changes in the thickness of the alpha plates. The globularization kinetics observations suggest that the controlling mechanism may be a form of 'geometric' recrystallization (Doherty *et al*. 1997). In this context, it is of interest to note that the onset of globularization occurs at strain levels (of about 1.0) at which a large fraction of the lamellae has rotated to orientations perpendicular to the compression axis. The development of

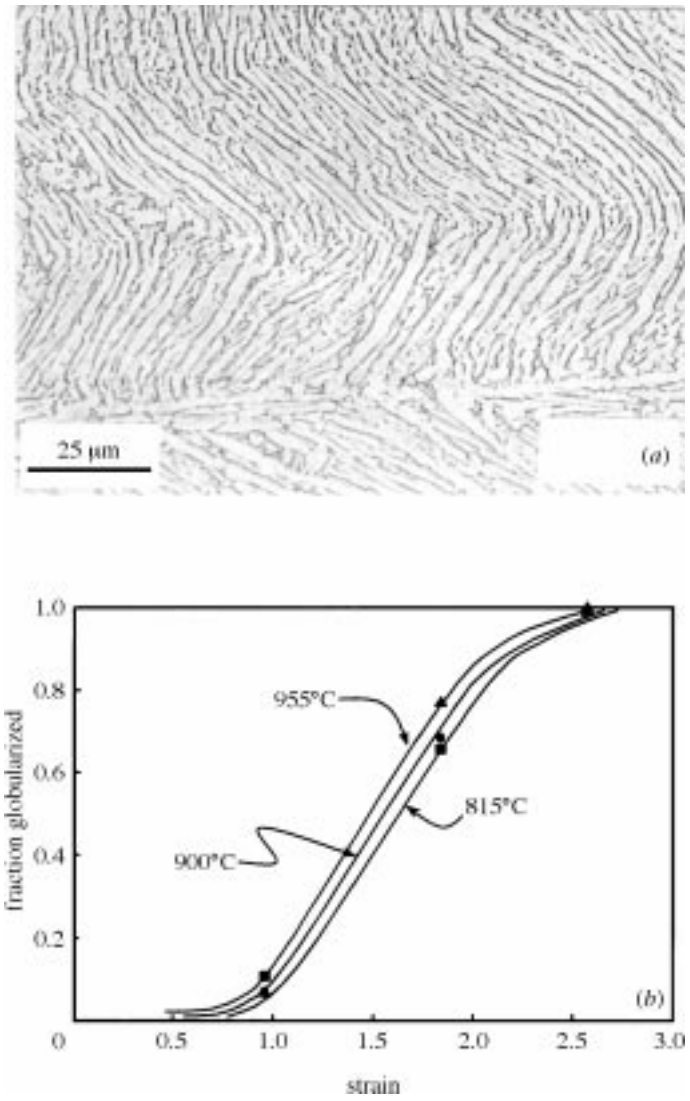

Figure 7. Platelet kinking and dynamic globularization of Ti–6Al–4V with a lamellar colony microstructure: (*a*) micrograph illustrating kinking and globularization nucleation from a test at 0.001 s^{-1}, 900 °C; and (*b*) fraction globularized versus strain for tests conducted at 0.001 s^{-1}.

sharp microstructural and crystallographic textures may accelerate the formation of microscopic translamellar shear bands (Weiss *et al*. 1985) that may provide the interfaces that are required for the 'pinch-off', which characterizes the geometric recrystallization process.

(iv) *Flow softening due to texture changes*

A final possibility to explain the non-heating-related flow softening observed in the flow curves for Ti–6Al–4V with the lamellar colony microstructure is a change in crystallographic texture. Texture influences may arise as a result of not only the

specific slip systems activated in the alpha and beta phases, but also the distribution of strain between the two phases and interphase interface sliding as a function of colony orientation. An adequate approach to predicting the Taylor factors (M) for the hot working of two-phase lamellar alloys is still under development (Dao *et al.* 1996; Lebensohn & Canova 1997). However, polycrystalline plasticity calculations for the hexagonal alpha phase reveal that both basal and prism slip tend to give rise to texture *hardening* during compression of a material with the starting texture shown in figure 1*b* (T. R. Bieler & S. L. Semiatin 1998, unpublished research). By contrast, pyramidal slip does produce texture *softening* during compression. On the other hand, pyramidal slip is predicted to produce *hardening* during uniaxial tension deformation, a result that conflicts with the flow-softening response deduced from load–elongation curves measured during hot tension tests (R. M. Miller & S. L. Semiatin 1997, unpublished research; Dowson *et al.* 1998). Needless to say, additional work is needed to assess the interaction of platelet bending and kinking on flow softening.

4. Plastic flow and microstructure evolution: Ti–45.5Al–2Cr–2Nb

The plastic flow behaviour and microstructure evolution for the lamellar gamma titanium aluminide Ti–45.5Al–2Cr–2Nb shows some similarities and some differences compared with the characteristics of hot-worked Ti–6Al–4V noted above. The discussion for the titanium aluminide alloy is addressed in separate sections on constitutive behaviour, flow-softening mechanisms, and microstructure evolution.

(*a*) *Constitutive behaviour*

The flow curves for the Ti–45.5Al–2Cr–2Nb alloy also exhibit a peak stress at very low strains, substantial flow softening, and an asymptotic approach to steady-state flow (Seetharaman & Semiatin 1999). Typical data for tests at 1095 °C (*ca.* 30 °C below the ordering temperature for alpha → alpha-two), shown in figure 8, show a strong dependence of flow stress on strain rate and, unlike Ti–6Al–4V, a very marked dependence on grain/colony size.

The peak flow stress $\bar{\sigma}_{\mathrm{p}}$ exhibits power-law relationships with $\dot{\bar{\varepsilon}}$ and grain size; thus, it is useful to analyse these data in terms of a generalized constitutive equation for hot deformation (Frost & Ashby 1982; Courtney 1990):

$$\dot{\bar{\varepsilon}} = C(D_{\mathrm{v}}GB/kT)(\bar{\sigma}/G)^n(b/d)^p, \tag{4.1}$$

where C is a constant, D_{v} is the volume diffusivity, G is the shear modulus, b is the Burgers vector of mobile dislocations, k is Boltzmann's constant, T is the temperature, $\bar{\sigma}$ is the flow stress, n is the stress exponent, d is the grain size, and p is the grain size exponent of the strain rate. At 1095 °C, the following values of physical and mechanical properties apply: $G = 56.6$ GPa (Lipsitt *et al.* 1975); $D_{\mathrm{v}} = 1.5 \times 10^{-4} \exp\{-291\,000/RT\}\ \mathrm{m^2\,s^{-1}}$ (Kroll *et al.* 1992); $k = 1.38 \times 10^{-23}\ \mathrm{J\,K^{-1}\,atom^{-1}}$; and $b = 2.8 \times 10^{-10}$ m. Figure 9*a* is a double logarithmic plot of the normalized deformation rate ($\dot{\bar{\varepsilon}}kT/DG_{\mathrm{v}}b$) against normalized peak stress ($\bar{\sigma}_{\mathrm{p}}/G$) for different values of prior-alpha grain/colony size d. Values of n obtained from the slopes of these plots range from 4.3 to 5.7. These data suggest that dislocation glide/climb processes control the rate of deformation (Frost &

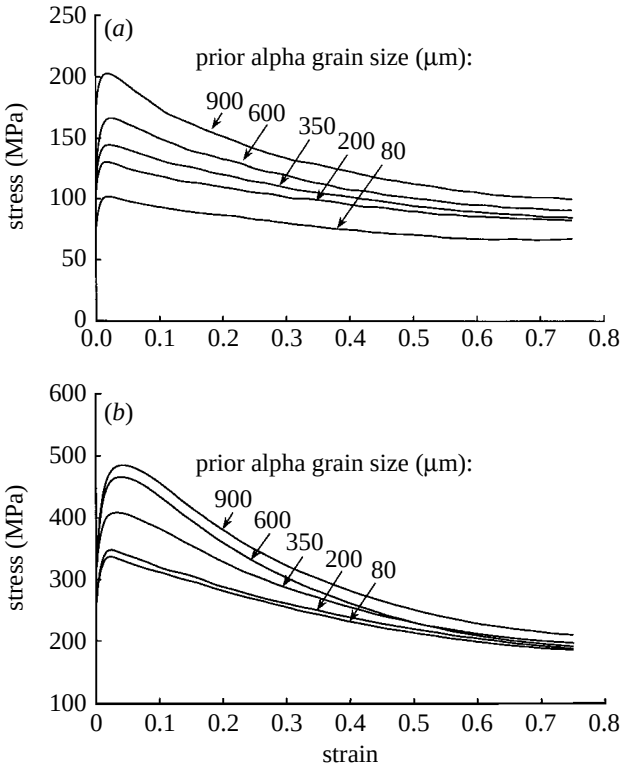

Figure 8. Flow curves from hot compression tests on Ti–45.5Al–2Cr–2Nb with various grain/colony sizes deformed at 1095 °C and constant strain rates of (*a*) 0.001 s^{-1} or (*b*) 0.1 s^{-1}.

Ashby 1982; Courtney 1990). On the other hand, double logarithmic plots of peak stress versus grain size reveal a dependence of approximately $\bar{\sigma}_p \sim d^q$, where $q = 0.2$ (figure 9*b*). Because $q = p/n$, this yields a value of the grain size exponent, $p = qn$, of approximately 1.0.

The large value of the stress exponent $n \approx 5$, rather than a value of 1–2, which would be expected when grain-boundary sliding/deformation processes become important, suggests that plastic flow for the titanium aluminide alloy conforms to a mixed mode of matrix and grain-boundary deformation. Such core–mantle-type deformation (Gifkins 1982; Mayo & Nix 1989; Springarn & Nix 1978) allows variations in n from 2 to 5 and in p from -3 to $+1$. The source of the grain-boundary deformation lies in the occurrence of a thin layer of gamma (plus B2) along the lamellar boundaries. If this layer is softer than the lamellae, then plastic deformation may localize in this layer, with the grain interiors contributing little to the total strain. Furthermore, as fine equiaxed grains form along the boundaries as a result of strain-induced globularization, the tendency for strain localization may become severe.

Although dynamic globularization occurs at comparatively low strains, as will be discussed below, the value of the strain-rate sensitivity varies very little with strain. In general, very fine globular microstructures, such as those developed during hot deformation of the titanium aluminide alloy, exhibit higher rate sensitivities at low-

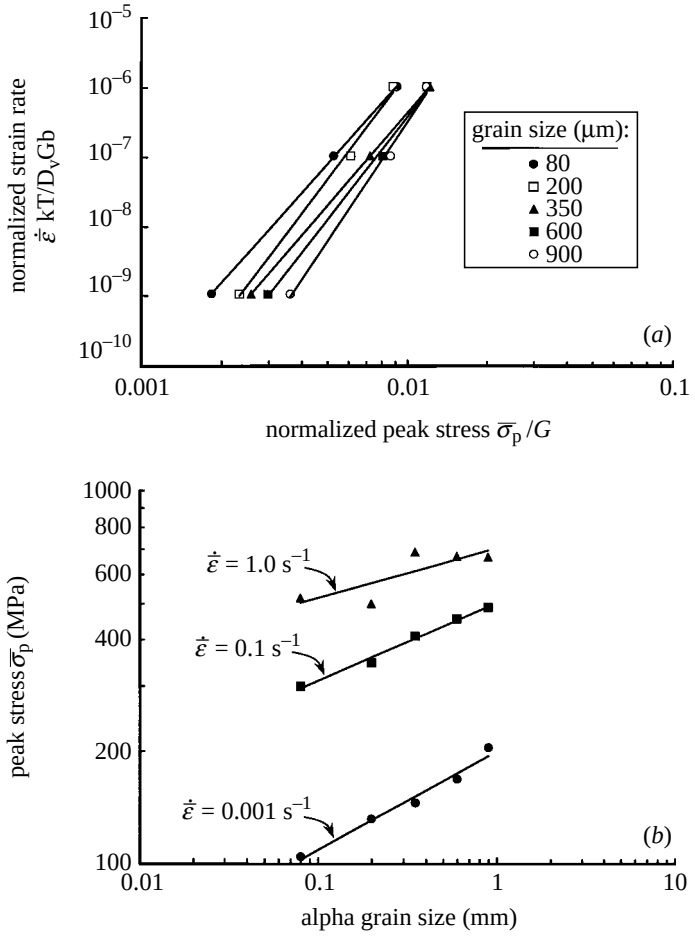

Figure 9. Peak flow stress data from hot compression tests on Ti–45.5Al–2Cr–2Nb: (*a*) normalized strain rate versus normalized peak stress; (*b*) peak stress versus colony/grain size.

to-moderate strain rates (*ca.* 0.001–0.1 s^{-1}) than do lamellar microstructures. The absence of such a trend for this material warrants further investigation.

(*b*) *Flow-softening mechanisms*

The flow softening observed in the flow curves for the Ti–45.5Al–2Cr–2Nb alloy may be attributed to two primary mechanisms: microbuckling/texture effects at low strains; and dynamic globularization at high strains (figure 10). Microbuckling is a manifestation of the high degree of deformation anisotropy in the lamellar gamma structure (Inui *et al.* 1992). At extremely low strains ($\varepsilon < 0.01$), gamma lamellae oriented for the easy mode of slip are strained. This is followed by the hard mode of slip involving translamellar shear in lamellae, which are oriented parallel or perpendicular to the compression axis. Continued straining, kinking/buckling of the lamellae by slip and twinning converts unfavourably oriented lamellae into favourable orientations, causing a net reduction in the flow stress. The reduction in flow stress resulting

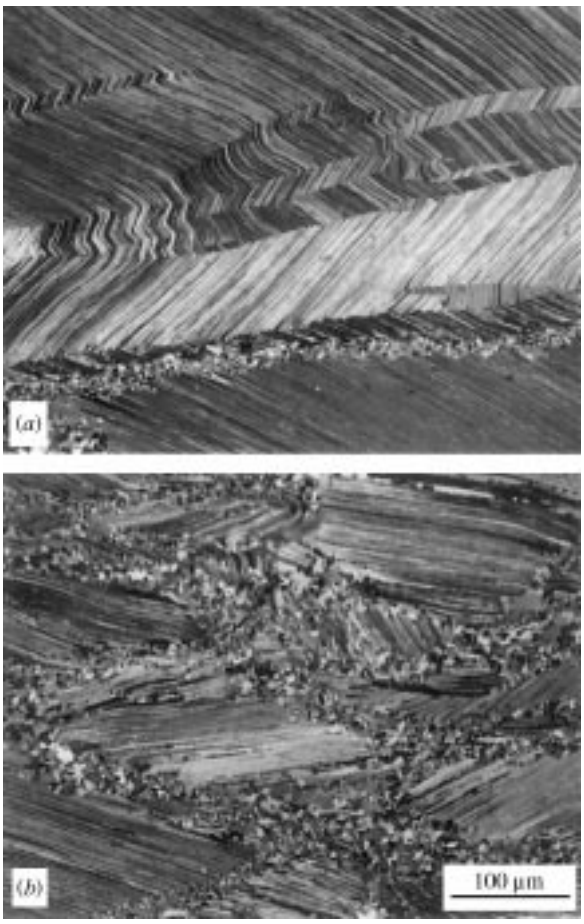

Figure 10. Polarized light micrographs illustrating kinking and globularization of the lamellar microstructure in Ti–45.5Al–2Cr–2Nb with an initial grain/colony size of 600 μm subjected to hot compression at 0.001 s^{-1}, 1095 °C and axial effective strains of (*a*) 0.3 or (*b*) 0.6.

from dynamic globularization is related to the size and volume fraction of the globular structure. At high strain rates, the globular structure is extremely fine, but the kinetics of the transformation is sluggish. In contrast, low strain rates are conducive to faster globularization kinetics, but lead to an increase in the average size of the globular grains. However, it is important to note that the maximum amount of flow softening occurs in the strain interval $0.05 \leqslant \varepsilon \leqslant 0.3$ (figure 8). While microbuckling is frequent in this strain range, the volume fraction of the globular grains is quite low. Thus, it may be conjectured that dynamic globularization plays a secondary role in the flow-softening process, similar to the behaviour found for Ti–6Al–4V. The development of a quantitative understanding of the effects of kinking and globularization on the flow-curve response would be a very valuable area of future research.

(*c*) *Dynamic globularization mechanism and kinetics*

As suggested by the micrographs in figure 10, lamellar grain boundaries act as the preferred sites for nucleation of the globular constituents in the early stage of defor-

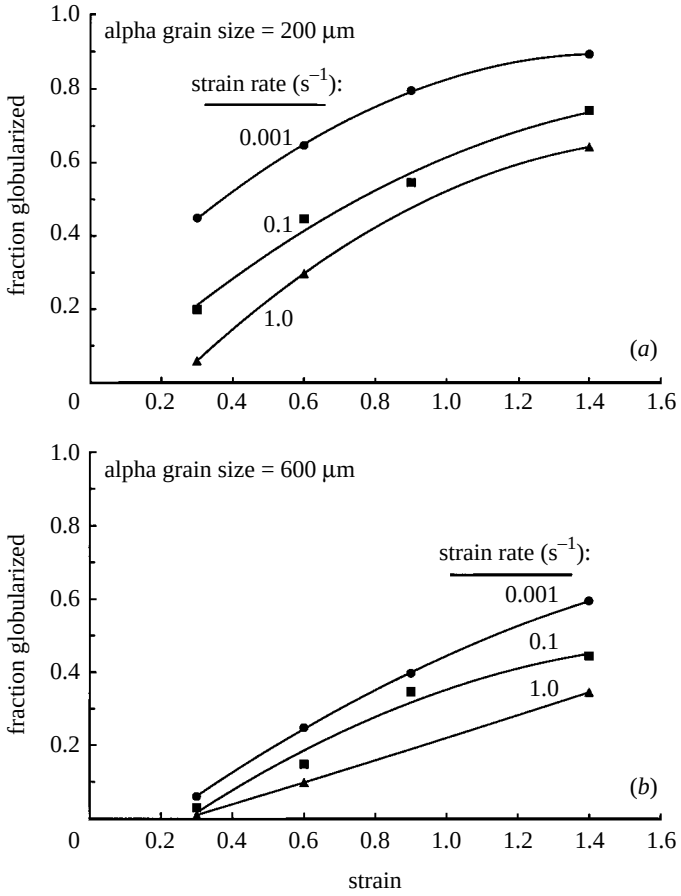

Figure 11. Fraction globularized versus strain plots determined via hot compression at 1095 °C and various strain rates on Ti–45.5Al–2Cr–2Nb samples with initial grain/colony sizes of (*a*) 200 μm or (*b*) 600 μm.

mation. The importance of grain boundaries as the nucleation sites increases with an increase in grain/colony size. As strain increases, kink bands characterized by severe localized strain become secondary sites for nucleation of the globules. Moreover, dynamically globularized grains grow only to a very limited extent, leading to significant grain refinement. This is followed by another cycle of nucleation and growth at the interface between the globularized grains and the untransformed lamellae. This type of repeated nucleation and growth leads to a steady advancement of the interface between the globularized and unglobularized regions towards the centre of the grains. These observations in the Ti–45.5Al–2Nb–2Cr alloy are very similar to those made by Sah *et al*. (1974) and Roberts *et al*. (1979) for dynamic recrystallization of nickel and an austenitic stainless steel, respectively. Nucleation of globular grains on kink bands or twin boundaries causes a break-up of the lamellar grains into smaller isolated units. This leads to an apparent reduction in the size of the lamellar colonies.

Figure 11 summarizes the influence of the lamellar grain size and strain rate on the fraction globularized. The data show that the globularized volume fraction decreases

sharply with grain size and strain rate. It is important to note that at typical isothermal forging conditions ($\dot{\varepsilon} \approx 0.001\ \mathrm{s}^{-1}$, $T \approx 1100$–$1150\ ^{\circ}\mathrm{C}$), cast + hot isostatically pressed (HIPed) titanium aluminide alloys will globularize only up to *ca.* 60%, and, thereafter, the rate of globularization becomes very sluggish. Apparent saturation of the fraction globularized at values well below unity during isothermal, hot deformation can be attributed to

(1) the continuous rotation of the lamellae until they become nearly perpendicular to the compression axis; and

(2) the associated decrease in plastic flow within the remnant colony.

Moreover, strain localization in the soft globularized region leads to very little additional accumulation of strain in the untransformed lamellae. The inability to achieve complete globularization via uniaxial deformation has spurred new research efforts directed towards the study of multi-step forging with a change in the orientation of the billet between the steps.

The measured globularization kinetics leads to Avrami exponents of the order of 1.1, or a value similar to that predicted by the model of Roberts *et al.* (1979), which treats repeated nucleation of new grains at the reaction front during dynamic recrystallization of austenitic stainless steel. Such agreement may be fortuitous because of several important differences between the plastic flow and evolution of microstructure for the two alloy systems. For example, the peaks in the flow curves of the lamellar titanium aluminide alloys are relatively sharp and occur at fairly low strain levels; the flow-softening rates observed beyond the peak stress are much higher than those reported for dynamic recrystallization of single-phase austenite. In addition, the micromechanisms of the nucleation event differ significantly. Nucleation of dynamic recrystallization in single-phase alloys occurs at pre-existing high-angle boundaries via the well-known mechanism of Bailey & Hirsch (1962), which involves local strain-induced grain-boundary migration. In contrast, the dynamic globularization process involves localized shear deformation at or near the grain/colony boundaries and in the kink bands. According to Wert & Bartholomeusz (1996), the lamellae seem to undergo fragmentation within these shear zones, followed by the flow of the softer phase around the fragments. Admittedly, the nucleation mechanisms for dynamic globularization are not yet fully established. Careful characterization of the grain-boundary regions of the lamellar structures by TEM and microtexture measurements is necessary to obtain a complete understanding of the initiation mechanism(s) of dynamic globularization.

5. Defect formation

The formation of defects during primary hot working may restrict the selection of processing variables, particularly for titanium and titanium aluminide alloys with lamellar colony microstructures. Therefore, the development of an understanding of workability as well as plastic flow and microstructure evolution is very important. The two most common types of defects are shear localization and cavitation.

(*a*) *Shear localization*

Shear localization is most common during plane-strain modes of deformation. During isothermal processes, high rates of flow softening and low values of the strain-

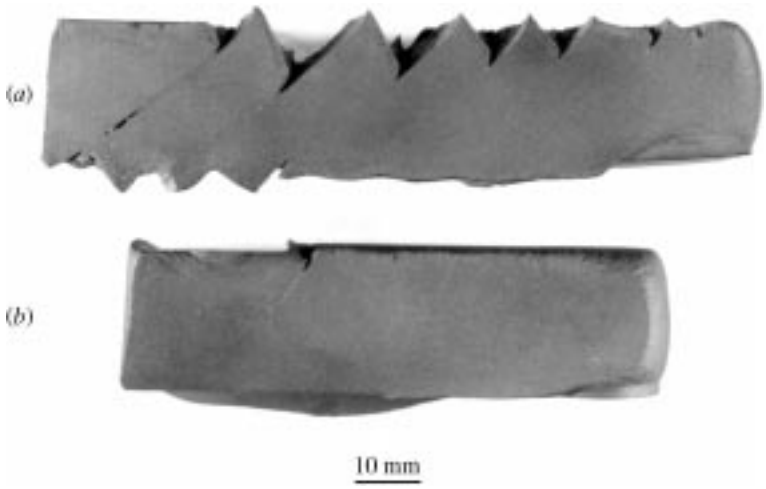

Figure 12. Macrographs of Ti–6Al–4V samples following equal channel angular extrusion at 900 °C (*a*) without or (*b*) with an initial increment of upsetting deformation.

rate sensitivity index promote shear banding (Semiatin & Jonas 1984). During non-isothermal (conventional) hot working, the tendency for non-uniform flow is affected by these parameters as well, but may be exacerbated by heat transfer and the development of large temperature gradients. Hence, an understanding of constitutive behaviour, including the temperature dependence of the flow stress, is extremely important.

Two examples, one for Ti–6Al–4V and one for Ti–45.5Al–2Cr–2Nb, will serve to illustrate the importance of material properties in process design to avoid shear localization. Both pertain to conventional hot deformation via the equal channel angular extrusion (ECAE) process. Developed in the former Soviet Union by Segal and co-workers (Segal *et al*. 1981; Segal 1992), ECAE comprises the deformation of prismatic bars/billets through two equal-area channels that intersect at an angle 2ϕ to each other. As the workpiece passes through the channels, it undergoes a simple shear whose magnitude is a function of the channel angle 2ϕ (Segal *et al*. 1981; Segal 1992; Iwahashi *et al*. 1996). The principal advantage of ECAE is the ability to impart very large deformations by passing the workpiece through the tooling multiple times, thereby obviating the need to melt large ingots to get a semi-finished product with a fine-wrought microstructure. On the other hand, the simple shear nature of the deformation can promote shear banding and shear fracture.

Figure 12 illustrates the behaviour of Ti–6Al–4V preforms (with a microstructure identical to that in figure 1*a*) during ECAE at 900 °C and a strain rate of *ca.* $2\ \mathrm{s}^{-1}$ using tooling with $2\phi = 90°$ (Semiatin & DeLo 1999). A die angle of 90 °C imparts an effective strain of approximately 1.15 during uniform flow. The sample in figure 12*a* was machined to fit snugly in the square container prior to extrusion. Thus, the metal flow through the die consisted solely of shear deformation. In this case, the flow localization tendency as quantified by the 'alpha' parameter in simple shear α_{ss} (equivalent to the ratio of normalized flow-softening rate γ' to strain-rate sensitivity m (see Semiatin & Jonas 1984)) is quite large, and shear failure occurs. By contrast, uniform flow (for the sample shown in figure 12*b*) was achieved by extruding a *round* preform. Use of such a preform geometry resulted in an upsetting-type deformation at

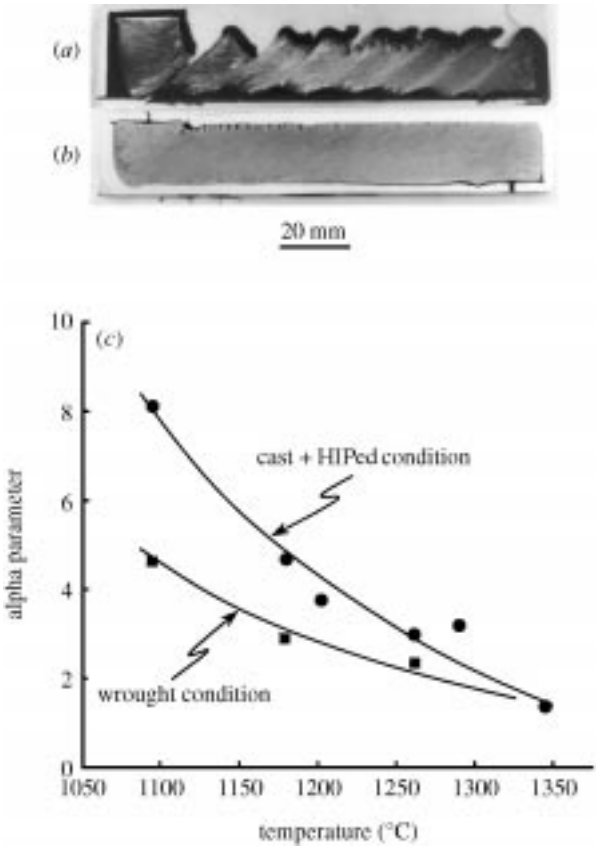

Figure 13. Macrographs of Ti–45.5Al–2Cr–2Nb samples following equal channel angular extrusion at (*a*) 1150 °C or (*b*) 1250 °C. The flow localization tendencies of this alloy are illustrated in the plot shown in (*c*).

low strains, at which the flow-softening rate is greatest (figure 3). During upsetting, the alpha parameter is lower (equal to $(\gamma' - 1)/m$), thereby stabilizing the flow. The flow-softening rate *following* the increment of upsetting deformation is lower, thus giving rise to a lower value of α_{ss} and uniform deformation as the workpiece passes through the shear zone in the ECAE die.

Similar results were found for cast + HIPed Ti–45.5Al–2Cr–2Nb with a lamellar microstructure having a grain/colony size of 150 μm. ECAE of canned samples of this material resulted in shear failure or uniform flow for processing conducted at 1150 °C or 1250 °C, respectively (figure 13*a*, *b*). These observations can also be explained, at least qualitatively, by using flow stress data to estimate the magnitude of α_{ss} for the alloy (figure 13*c*; and see Semiatin *et al*. (1995)). The application of FEM modelling is now providing additional insight into the effects of both material properties and heat transfer on flow localization during ECAE (DeLo & Semiatin 1999).

(*b*) *Cavitation*

Despite being largely compressive in nature, bulk hot-working operations such as forging, extrusion, etc., often give rise to secondary tensile stresses that may lead to

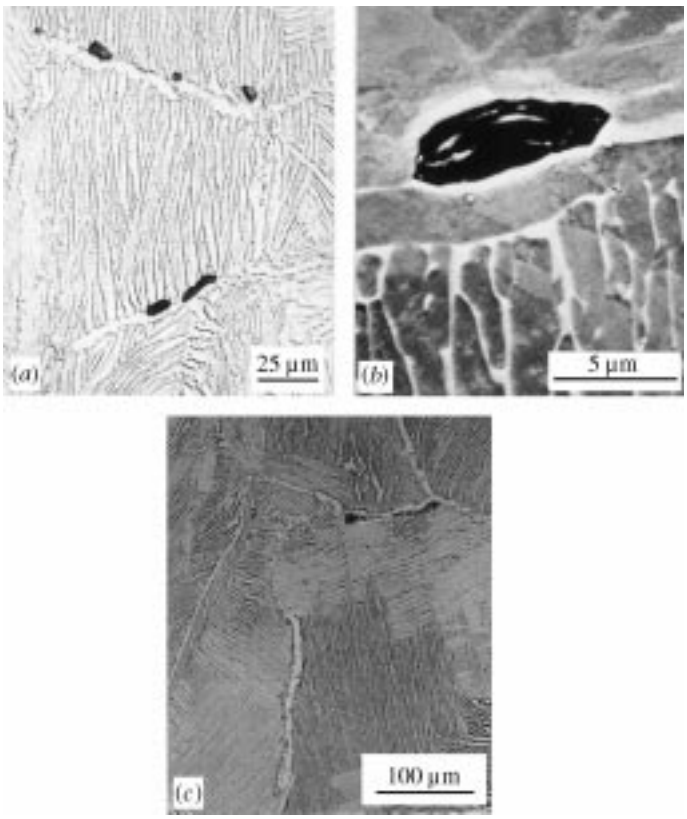

Figure 14. Cavitation observations for Ti–6Al–4V samples with a lamellar colony microstructure deformed at *ca.* 0.1 s^{-1}, 815 °C under conditions of (*a*), (*b*) uniaxial tension or (*c*) pancake forging. The micrograph in (*c*) was taken near the barrelled free surface of the pancake.

cavitation and fracture. Secondary tensile stresses may result from geometry, friction, flow non-uniformity and other sources. Even if fracture does not occur, the presence of damage if not healed during secondary processing may be deleterious to service properties. Such problems can be especially troublesome when the defects are internal and not easily detected by non-destructive inspection techniques. The discussion here illustrates some of the features of cavitation during hot working of Ti–6Al–4V with the lamellar colony microstructure. Research on cavitation during hot working of gamma titanium aluminide alloys has been conducted by Seetharaman & Semiatin (1996, 1998).

Research on cavitation in Ti–6Al–4V has focused on the mechanisms, phenomenology and modelling of the failure process. During uniaxial tension, testing at temperatures of *ca.* 900 °C and lower, the 'initiation' of cavities (observable at 500×) occurs at low strains (less than about 0.2) in very thin layers (*ca.* 0.2 μm) of beta that lie between the grain-boundary alpha and the terminus of packets of lamellar alpha (figure 14). The degree of incompatibility and the level of hydrostatic tensile stresses generated in the soft beta layer appear to be highest when

(1) the maximum principal (tensile) stress lies perpendicular to the grain boundary; and

(2) the corresponding lamellar alpha plates on at least one side of the grain boundary are parallel to this stress (Semiatin *et al*. 1998*b*).

At higher temperatures (e.g. 955 °C), cavity 'initiation' occurs at substantially larger strains due to increasing proportions of ductile beta phase in the colony alpha structure and, hence, increased diffusional accommodation; cavity initiation thus takes place in a partly globularized microstructure by fracture of remnant alpha plates. This variation of cavity initiation strain with temperature, coupled with moderate-to-high cavity growth rates, leads to a 'trough' in the tensile reduction-in-area versus temperature (Semiatin *et al*. 1998). The cavity initiation and growth modes under complex stress states, such as may be found in a forging, appear to be similar (figure 14). Furthermore, initial work (Semiatin *et al*. 1999) has shown that the cavity initiation and fracture phenomenology under these conditions can be correlated to uniaxial tension measurements using classical continuum approaches, such as that developed by Cockcroft & Latham (1966).

Micromechanical modelling is now providing further insight into the influence of material properties, local and far-field stress state, and defects on cavitation (Ghosh & Semiatin 1999). The application of a diffusional cavity growth model for Ti–6Al–4V with a lamellar colony microstructure is inappropriate for several reasons. Firstly, cavities in Ti–6Al–4V are not observed to be spherical nor to be distributed uniformly, as noted above, unlike the assumptions of diffusion-controlled cavitation models. In addition, diffusion models often assume an initial size that satisfies a surface-energy condition. However, such a surface-energy consideration requires stresses for early growth that are unrealistically high. Lastly, the diffusion rates at low to moderate temperatures in the hot-working regime for Ti–6Al–4V are too low to contribute significantly to the rapid initial growth of nanoscale cavities. Because of these deficiencies, a constrained plasticity analysis for the early as well as later stages of growth has been formulated. For nanoscale cavities that originate from a vacancy cluster, for instance, local plasticity may begin from the glide of a few discrete dislocations or the climb of a few atom planes. As the void volume increases, general plastic flow involving many dislocations is expected.

For Ti–6Al–4V, the colony portion of the microstructure has a flow stress approximately two to three times that of the thin beta layer lying at the grain boundaries, thereby inducing a much higher local strain rate in the beta layer. When the cavity is very small (relative to the thickness of the alpha plate), a zone of very high deformation extends to a distance of approximately 10 times the cavity diameter, and growth is largely dilatational in nature. As the cavity grows to a size exceeding the alpha-plate thickness, the level of constraint is less, the region of high local strain rate decreases to an extent approximately equal to the cavity diameter, and cavity growth occurs via 'conventional' plasticity, principally in the direction of the applied stress.

Typical finite-difference-method predictions of cavity diameter (equivalent to the diameter of a spherical cavity having the same volume as that of the actual cavity) for Ti–6Al–4V are shown in figure 15. The change in cavity dimension from nanometre to near-micron size occurs rapidly due to constrained plasticity, but the subsequent conventional-plasticity growth rate is substantially slower. The rate of growth in both regimes decreases with temperature due to corresponding increases in the strain-rate sensitivity m. The results also reveal that the growth parameter for a single cavity

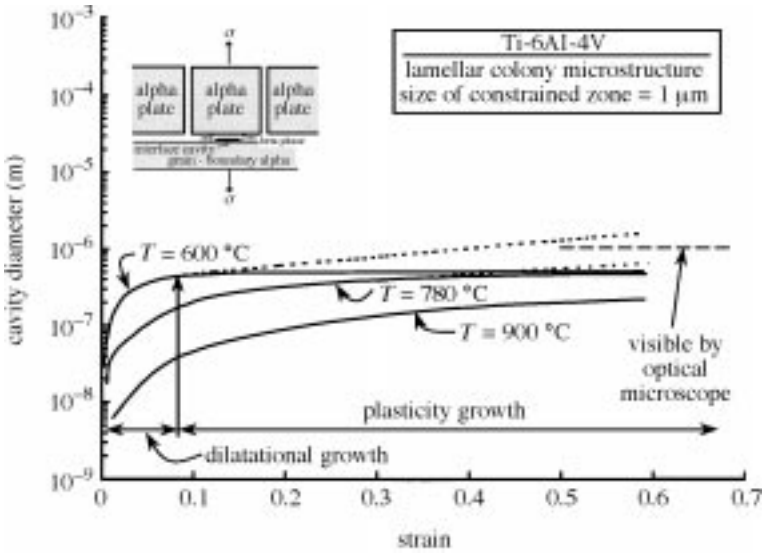

Figure 15. Plasticity analysis predictions of the diameter of an intergranular cavity as a function of axial strain for a Ti–6Al–4V sample with a lamellar colony microstructure subjected to uniaxial tensile deformation.

($\eta \sim \mathrm{d}\ln r/\mathrm{d}\varepsilon$, where r denotes the cavity radius) can vary widely depending on the growth stage. Specifically, when the cavity size is large enough to be detected in the optical microscope (i.e. 'initiation' has occurred in an operational sense), growth via constrained plasticity is usually over, and, thus, reported values of η are those characteristic of growth by conventional plasticity. The constrained plasticity analysis is also capable of elucidating the effect of a *size distribution* of second-phase constituents/imperfections on the transition strains from dilatational to plasticity growth. By this means, a range of cavity sizes that may mirror experimental observations may be predicted. These cavity size distributions are often attributed to continuous nucleation rather than to variations in the rate of growth, to the point of becoming microscopically detectable.

6. Future directions

The broad features of the primary hot-working behaviour of alpha/beta titanium and gamma titanium aluminide alloys with lamellar colony microstructures have been described. Although the phenomenology of plastic flow has been extensively investigated, much work remains to document and quantify the mechanisms that underlie microstructure and texture evolution, and to correlate such mechanisms to phenomenological descriptions. To this end, a number of areas for future research on lamellar titanium alloys can be identified, including the following.

(1) TEM studies of substructure evolution during hot working (and subsequent annealing) to establish deformation mechanisms, strain partitioning between phases, etc.

(2) TEM investigation of globularization mechanisms.

(3) Micromechanical modelling of the globularization process.

(4) Effect of strain path on flow phenomenology/mechanisms and globularization kinetics; use of this understanding to design optimal ingot-breakdown processes.

(5) Texture evolution and platelet kinking during hot working (and subsequent annealing), and their effect on flow phenomenology.

(6) State variable modelling of constitutive behaviour.

(7) Development and validation of micromechanical models for failure under complex stress states and arbitrary strain paths.

This work was conducted as part of the in-house research of the Processing Science Group of the Materials and Manufacturing Directorate, Air Force Research Laboratory (formerly the Wright Laboratory). The support of the in-house programme by directorate management and the Air Force Office of Scientific Research (C. Ward, S. Wu, programme managers) is gratefully acknowledged. Two of the authors were supported under the auspices of Air Force contracts F33615-96-C-5251 (V.S.) and F33615-94-C-5804 (A.K.G.). Technical discussions with D. DeLo and the assistance of N. Frey, P. Fagin and E. Shell in performing the experimental work, and L. A. Farmer in preparing the manuscript, are also greatly appreciated.

References

Bailey, J. E. & Hirsch, P. B. 1962 The recrystallization process in some polycrystalline metals. *Proc. R. Soc. Lond.* A **267**, 11–30.

Briottet, L., Jonas, J. J. & Montheillet, F. 1996 A mechanical interpretation of the activation energy of high-temperature deformation in two-phase materials. *Acta Mater.* **44**, 1665–1672.

Cockcroft, M. G. & Latham, D. J. 1966 A simple criterion of fracture for ductile metals. National Engineering Laboratory report no. 240, East Kilbride, Glasgow, Scotland.

Cope, M. T. & Ridley, N. 1986 Superplastic deformation characteristics of microduplex Ti–6Al–4V alloy. *Mater. Sci. Technol.* **2**, 140–145.

Courtney, T. H. 1990 *Mechanical behavior of materials*. New York: McGraw-Hill.

Dao, M., Kad, B. & Asaro, R. J. 1996 Deformation and fracture under compressive loading in lamellar TiAl microstructures. *Phil. Mag.* A **74**, 569–591.

DeLo, D. P. & Semiatin, S. L. 1999 Finite element modeling of nonisothermal equal channel angular extrusion. *Metall. Mater. Trans.* A **30**. (In the press.)

Doherty, R. D., Hughes, D. A., Humphreys, F. J., Jonas, J. J., Jensen, D. J., Kassner, M. E., King, W. E., McNelley, T. R., McQueen, H. J. & Rollett, A. D. 1997 Current issues in recrystallization: a review. *Mater. Sci. Engng* A **238**, 219–274.

Dowson, A. L., Blackwell, P., Jones, M., Young, J. M. & Duggan, M. A. 1998 Hot rolling and superplastic forming response of net shape processed Ti–6Al–4V produced by centrifugal spray deposition. *Mater. Sci. Technol.* **14**, 640–650.

Frost, H. J. & Ashby, M. F. 1982 *Deformation-mechanism maps*. Oxford: Pergamon.

Ghosh, A. K. & Semiatin, S. L. 1999 An analysis of cavity nucleation and early growth during hot deformation. *Acta Mater.*

Gifkins, R. C. 1982 Mechanisms of superplasticity. In *Superplastic forming of structural alloys* (ed. N. E. Paton & C. H. Hamilton), pp. 3–26. Warrendale, PA: The Metallurgical Society of AIME.

Goetz, R. L. & Seetharaman, V. 1998 Modeling dynamic recrystallization using cellular automata. *Scr. Mater.* **38**, 405–413.

Humphreys, F. J. & Hatherly, M. 1995 Recrystallization and related phenomena. Oxford: Elsevier.

Inui, H., Oh, M. H., Nakamura, A. & Yamaguchi, M. 1992 Room temperature tensile deformation of polysynthetically twinned (PST) crystals of TiAl. *Acta Metall. Mater.* **40**, 3095–3104.

Iwahashi, Y., Wang, J., Horita, Z., Nemoto, M. & Langdon, T. G. 1996 Principle of equal-channel angular pressing for the processing of ultrafine grain materials. *Scr. Mater.* **35**, 143–147.

Jonas, J. J. & McQueen, H. J. 1975 Recovery and recrystallization during high temperature deformation. In *Treatise on materials science. Vol. 6. Plastic deformation of materials* (ed. R. J. Arsenault), pp. 394–490. New York: Academic.

Jonas, J. J., Sellars, C. M. & McG. Tegart, W. J. 1969 Strength and structure under hot-working conditions. *Metall. Rev.* **14**, 1–24.

Kaibyshev, O. A., Valitov, V. A. & Salishchev, G. A. 1993 The effect of phase state and conditions of hot deformation on the formation of microduplex structure in a high-temperature nickel alloy. *Phys. Metals Metallog.* **75**, 409–414.

Korshunov, A. A., Enikeev, F. U., Mazurskii, M. I., Salishchev, G. A., Muravlev, A. V., Chistyakov, P. V. & Dimitriev, O. O. 1994 Effect of method of high temperature loading on transformation of lamellar structure in VT9 titanium alloy. *Russ. Metall.* **3**, 103–108.

Kroll, S., Mehrer, H., Stolwijk, N. A., Herzig, C., Rosenkranz, R. & Frommeyer, G. 1992 Titanium self-diffusion in the intermetallic compound γ-TiAl. *Z. Metallk.* **83**, 591–595.

Laasraoui, A. & Jonas, J. J. 1991 Recrystallization of austenite after deformation at high temperatures. *Metall. Trans.* A **22**, 151–160.

Lebensohn, R. A. & Canova, G. R. 1997 A self-consistent approach for modeling texture development of two-phase polycrystals: application to titanium alloys. *Acta Mater.* **45**, 3687–3694.

Lipsitt, H. A., Schectman, D. & Schafrik, R. E. 1975 The deformation and fracture of TiAl at elevated temperatures. *Metall. Trans.* A **6**, 1991–1996.

Lombard, C. M., Goetz, R. L. & Semiatin, S. L. 1993 Numerical analysis of the hot tension test. *Metall. Trans.* A **24**, 2039–2047.

Malcor, J. G., Montheillet, F. & Champin, B. 1985 Mechanical and microstructural behavior of Ti–6Al–4V in the hot working range. In *Titanium: science and technology* (ed. G. Luetjering, U. Zwicker & W. Bunk), pp. 1495–1502. Oberursel, Germany: Deutsche Gesellschaft für Metallkunde e. V.

Matsumoto, T., Nishigaki, M., Fukuda, M. & Nishimura, T. 1985 Effect of heat treatment on the surface defect and mechanical properties of Ti–6Al–4V rolled bar. In *Titanium: science and technology* (ed. G. Luetjering, U. Zwicker & W. Bunk), pp. 617–623. Oberursel, Germany: Deutsche Gesellschaft für Metallkunde e. V.

Mayo, M. J. & Nix, W. D. 1989 Direct observation of superplastic flow mechanisms in torsion. *Acta Metall.* **37**, 1121–1134.

Nadai, A. 1950 *Theory of flow and fracture of solids.* New York: McGraw-Hill.

Oh, S. I., Semiatin, S. L. & Jonas, J. J. 1992 An analysis of the isothermal hot compression test. *Metall. Trans.* A **23**, 963–975.

Roberts, W., Boden, H. & Ahlblom, B. 1979 Dynamic recrystallization kinetics. *Metal Sci.* **13**, 195–205.

Rollett, A. D. 1997 Overview of modeling and simulation of recrystallization. *Prog. Mater. Sci.* **42**, 79–99.

Rollett, A. D., Luton, M. J. & Srolovitz, D. J. 1992 Microstructural simulation of dynamic recrystallization. *Acta Metall. Mater.* **40**, 43–55.

Sah, J. P., Richardson, G. J. & Sellars, C. M. 1974 Grain size effects during dynamic recrystallization of nickel. *Metal Sci.* **8**, 325–331.

PHILOSOPHICAL TRANSACTIONS OF THE ROYAL SOCIETY A MATHEMATICAL, PHYSICAL & ENGINEERING SCIENCES

Seetharaman, V. & Semiatin, S. L. 1996 Influence of temperature transients on the hot workability of a two-phase gamma titanium aluminide alloy. *Metall. Mater. Trans.* A **27**, 1987–2004.

Seetharaman, V. & Semiatin, S. L. 1998 Intergranular fracture of gamma titanium aluminides under hot working conditions. *Metall. Mater. Trans.* A **29**, 1991–1999.

Seetharaman, V. & Semiatin, S. L. 1999 Effect of the lamellar grain size on plastic flow behavior and microstructure evolution during hot working of a gamma titanium aluminide alloy. *Metall. Mater. Trans.* A. (Submitted.)

Segal, V. M. 1992 Working of metals by simple shear deformation process. In *Proc. Fifth Int. Aluminum Technol. Seminar* **2**, 403–407.

Segal, V. M., Reznikov, V. I., Drobyshevkiy, A. E. & Kopylov, V. I. 1981 Plastic working of metals by simple shear. *Russ. Metall.* **1**, 99–105.

Sellars, C. M. 1990 Modeling microstucture development during hot rolling. *Mater. Sci. Technol.* **6**, 4133–4144.

Semiatin, S. L. & DeLo, D. P. 1999 Equal channel angular extrusion of difficult-to-work alloys. Air Force invention D00291, US patent allowance granted.

Semiatin, S. L. & Jonas, J. J. 1984 *Formability and workability of metals*. Materials Park, OH: ASM International.

Semiatin, S. L. & Lahoti, G. D. 1981 Deformation and unstable flow in hot forging of Ti–6Al–2Sn–2Zr–2Mo–0.1Si. *Metall. Trans.* A **12**, 1705–1717.

Semiatin, S. L., Thomas, J. F. & Dadras, P. 1983 Processing-microstructure relationships for Ti–6Al–2Sn–4Zr–2Mo–0.1Si. *Metall. Trans.* A **14**, 2363–2374.

Semiatin, S. L., Segal, V. M., Goetz, R. L., Goforth, R. E. & Hartwig, T. 1995 Workability of a gamma titanium aluminide alloy during equal channel angular extrusion. *Scr. Metall. Mater.* **33**, 535–540.

Semiatin, S. L., Seetharaman, V. & Weiss, I. 1997 Hot working of titanium alloys: an overview. In *Advances in the science and technology of titanium alloy processing* (ed. I. Weiss, R. Srinivasan, P. J. Bania, D. Eylon & S. L. Semiatin), pp. 3–73. Warrendale, PA: The Minerals, Metals and Materials Society.

Semiatin, S. L., Seetharaman, V., Ghosh, A. K., Shell, E. B., Simon, M. P. & Fagin, P. N. 1998 Cavitation during hot tension testing of Ti–6Al–4V. *Mater. Sci. Engng* A **256**, 92–110.

Semiatin, S. L., Goetz, R. L., Shell, E. B., Seetharaman, V. & Ghosh, A. K. 1999 Cavitation and failure during hot forging of Ti–6Al–4V. *Metall. Mater. Trans.* A **30**. (In the press.)

Shen, G., Semiatin, S. L. & Shivpuri, R. 1995 Modeling microstructural development during the forging of Waspaloy. *Metall. Mater. Trans.* A **26**, 1795–1803.

Springarn, J. R. & Nix, W. D. 1978 Diffusional creep and diffusionally accommodated grain rearrangement. *Acta Metall.* **26**, 1389–1398.

Suzuki, H. G. & Eylon, D. 1993 Hot ductility of titanium alloys—a comparison with carbon steels. *ISIJ Int.* **33**, 1270–1274.

Weiss, I. & Semiatin, S. L. 1998 Thermomechanical processing of beta titanium alloys—an overview. *Mater. Sci. Engng* A **243**, 46–65.

Weiss, I. & Semiatin, S. L. 1999 Thermomechanical processing of alpha titanium alloys—an overview. *Mater. Sci. Engng* A **263**. (In the press.)

Weiss, I., Welsch, G. E., Froes, F. H. & Eylon, D. 1985 Mechanisms of microstructure refinement in Ti–6Al–4V. In *Titanium: science and technology* (ed. G. Luetjering, U. Zwicker & W. Bunk), pp. 1503–1510. Oberursel, Germany: Deutsche Gesellschaft für Metallkunde e. V.

Wert, J. A. & Bartholomeusz, M. F. 1996 Effect of creep strain on microstructural stability and creep resistance of a $TiAl/Ti_3Al$ lamellar alloy. *Metall. Mater. Trans.* A **27**, 127–134.

Discussion

L. M. Brown (*Cavendish Laboratories, University of Cambridge, UK*). Do I have the correct picture? Plastic buckling of the lamellae can perhaps be regarded as what can occur in a fibre-reinforced material, where plastic inhomogeneity can rotate sections of fibre away from their maximally reinforcing orientation, causing very pronounced softening. It is 'buckling' but the plasticity of the surrounding soft matrix plays a key role. It is not the same thing as the plastic buckling of an isolated ligament.

S. L. Semiatin. Yes, this is correct. We would like to add that a group of lamellae (be they alpha plus beta lamellae in Ti–6Al–4V or alpha plus gamma lamellae in the gamma titanium aluminide alloys) does appear to undergo cooperative buckling such that the compatibility of strain across the lamellae is ensured.

M. J. Stowell (*Saffron Walden, Essex, UK*). Could what Dr Semiatin describes as 'micro shear banding' in the globularization process be grain-boundary sliding?

S. L. Semiatin. By the term 'micro shear banding', we are not implying that grain-boundary sliding is occurring. Rather, we mean that localization of strain occurs across a lamellar packet which may be along a crystallographic plane (e.g. formation of a deformation band), or a subgrain boundary. Such shear bands may give rise to offsets in the platelet due to plastic flow or matter transport where the shear band meets the alpha–beta interface. It is important to bear in mind that a number of these so-called micro shear bands must be formed within a given platelet in order to produce equiaxed grains rather than long rods.